AGU PUBLICATIONS

JGR

Journal of Geophysical Research: Atmospheres

RESEARCH ARTICLE
10.1002/2013JD021048

Special Section:
The 2011-12 Indian Ocean Field Campaign: Atmospheric-Oceanic Processes and MJO Initiation

Key Points:
- Explosive mesoscale convective system observed during MJO initiation in DYNAMO
- Vigorous equatorial low-pressure system provided favorable conditions
- Multiple convective systems reduced shear prior to explosive convective system

Supporting Information:
- Readme
- Animation S1

Correspondence to:
F. Judt,
fjudt@rsmas.miami.edu

Citation:
Judt, F., and S. S. Chen (2014), An explosive convective cloud system and its environmental conditions in MJO initiation observed during DYNAMO, *J. Geophys. Res. Atmos.*, *119*, 2781–2795, doi:10.1002/2013JD021048.

Received 15 OCT 2013
Accepted 17 FEB 2014
Accepted article online 21 FEB 2014
Published online 18 MAR 2014

An explosive convective cloud system and its environmental conditions in MJO initiation observed during DYNAMO

Falko Judt[1] and Shuyi S. Chen[1]

[1]Division of Meteorology and Physical Oceanography, Rosenstiel School of Marine and Atmospheric Science/University of Miami, Miami, Florida, USA

Abstract An unusually large, explosive convective cloud system was observed over the equatorial Indian Ocean on 28 November 2011 during the DYNAMO (Dynamics of the Madden-Julian Oscillation (MJO)) field campaign. The significance of this mesoscale convective system (MCS) is its size and explosive development of cold cloud tops (−96°C) during the initiation of a strong MJO event. Observations from the DYNAMO show that the large MCS developed within a well-defined synoptic-scale cyclonic circulation associated with an equatorial low-pressure system with characteristics of a mixed Rossby-gravity wave that dominated the flow in the DYNAMO array. Prior to the development of the MCS, the equatorial flow was characterized by strong vertical wind shear with low-level westerlies and upper level easterlies. A region of decreased wind shear and enhanced upper level divergence emerged concurrently with the passage of the westward moving mixed Rossby-gravity wave-related low-pressure system and convective activity. In situ sounding observations suggest that widespread deep convection upstream of the large MCS may have contributed to the reduction of the upper level easterlies through vertical momentum transport and convective outflow. Both the reduction in vertical wind shear and enhanced low-level convergence induced by the equatorial low-pressure system created a favorable environment for the rapid development of the MCS. This study examines the development of the MCS and the associated synoptic-scale equatorial low-pressure system within the large-scale MJO circulation using in situ sounding observations from DYNAMO, which provide new insights into the interaction between convection and environmental flow during MJO initiation over the equatorial Indian Ocean.

1. Introduction

One of the most challenging problems in prediction of the Madden-Julian Oscillation (MJO) [*Madden and Julian*, 1971, 1972] is the timing and structure of equatorial convection during MJO initiation over the Indian Ocean (IO). This shortcoming contributes to the limited predictive skill of the MJO and its downstream impacts in numerical weather prediction and climate models [e.g., *Lin et al.*, 2006; *Zhang et al.*, 2006; *Benedict and Randall*, 2009]. Some models struggle to predict the onset of convective activity over the IO, unless the initial conditions include some form of a preexisting convective MJO signal [e.g., *Lin et al.*, 2008; *Seo et al.*, 2009; *Nasuno*, 2013]. One of the reasons for the lack of skill is that some physical processes believed to play an important role in MJO initiation are not well understood and not represented in the models. For example, the intricate relationship between deep convective systems and the large-scale environmental flow may be important for MJO initiation. Observations from the recent DYNAMO (Dynamics of the Madden-Julian Oscillation) field campaign are used to shed new light on the interactions between organized deep convection and the large-scale environment during MJO initiation over the IO.

In the classic conceptual model of the MJO proposed by *Madden and Julian* [1972], the large-scale convective activity (active phase) is associated with the ascending branch of a planetary scale overturning zonal circulation. This large-scale equatorial zonal flow pattern composed of upper tropospheric easterlies and westerly flow in the lower levels causes strong vertical wind shear over a large area of the equatorial IO. Satellite observations in the equatorial IO and the west Pacific have shown that the convectively active phase of the MJO is characterized by multiscale variability and consists of convective cloud systems of various sizes [e.g., *Chen et al.*, 1996; *Yamada et al.*, 2010]. Westward propagating disturbances were found to exhibit characteristics of certain types of equatorial waves, such as equatorial Rossby waves or mixed Rossby-gravity

waves [*Wheeler and Kiladis*, 1999; *Yang*, 2011]. *Dunkerton and Crum* [1995] described prominent eastward propagating anomalies within the active phase of the MJO and related them to convectively coupled Kelvin waves. *Yamada et al*. [2010] documented westward propagating cloud clusters within an eastward propagating synoptic-scale disturbance in the IO. The size distribution and intensity of convective systems within the MJO active phase is also highly variable. *Chen et al*. [1996] and *Chen and Houze* [1997a] showed that the size distribution of convective systems in the MJO varies with large-scale environmental conditions on intraseasonal to interannual time scales. In a different study, *Chen and Houze* [1997b] showed that a prominent 2 day periodicity in convective activity is related to the diurnal cycle of organized deep convection over the tropical oceans during the MJO active phase. Some studies suggest that these multiscale processes are essential to producing an MJO event [e.g., *Moncrieff*, 2004; *Biello and Majda*, 2005].

Holloway et al. [2013] demonstrated that convection-environment interactions play an important role in convective organization and MJO eastward propagation, supporting previous hypotheses that highlighted the importance of multiscale interactions. *Kerns and Chen* [2014] showed that synoptic-scale features modulate the convective activity to a great degree and act to influence mesoscale organization. These recent studies suggest that interactions between organized convective systems and the large-scale flow may be an important contributor to MJO initiation. Prior to DYNAMO, the structure and evolution of convective systems within the large-scale convective envelope of the MJO were mostly unknown because previous studies often used some form of time and spatial averages, such as 5 day pentads [e.g., *Matthews*, 2008]. Studies based on observations from earlier field experiments indicated that organized convective systems play an important role in the redistribution of mass, momentum, and moisture. *Houze* [1977] and *Zipser* [1977] provided detailed observations about the structure and life cycles of mesoscale convective systems (MCSs) over the tropical oceans. *LeMone et al*. [1984] documented that deep convective cloud systems transport significant amounts of horizontal momentum vertically and are able to change the environmental flow in the upper levels. The upward momentum flux was determined to reduce the environmental vertical wind shear over and in the vicinity of the convective systems. Others have shown that large MCSs can transport westerly momentum into the lower levels and enhance the westerly surface winds associated with the MJO over the west Pacific [*Houze et al*., 2000; *Mechem et al*., 2006].

The DYNAMO field campaign was designed to better understand the physical processes affecting MJO initiation [*Zhang*, 2005]. One of the key questions regarding MJO initiation is how the widespread equatorial convection develops and interacts with the large-scale flow over the IO. Unprecedented in situ and remote sensing observations have been collected during DYNAMO in three distinct MJO initiation events over the IO from October 2011 to March 2012 [*Yoneyama et al*., 2013]. Multiple coordinated observing platforms, including sounding networks, cloud and precipitation radars, research ships, and aircraft gathered a plethora of atmospheric and oceanic data on a variety of scales in order to shed light on the question of interactions between convection and environment during MJO initiation.

This study describes the explosive development of a very large MCS over the equatorial IO and examines the interaction of organized convection and its environment. The word "explosive" here refers to the rapid expansion of cold cloud tops as observed by satellite infrared (IR) data. The convective system developed during the local afternoon and evening hours on 28 November 2011 and was part of a well-defined MJO initiation event during DYNAMO. We investigate how a synoptic-scale equatorial low-pressure system and multiple MCSs near the equator have likely contributed to the development of the rapidly evolving MCS by modulating the environmental flow. The large MCS in turn may have helped intensify the synoptic-scale low-pressure system and associated circulation.

Figure 1 shows an enhanced satellite IR image of the explosive convective cloud system that occurred on 28 November 2011 in the DYNAMO southern sounding array. This convective system was unique in its magnitude of cold IR cloud top temperatures (minimum reaching 177 K or −96°C), size, and rapid development during DYNAMO. It developed, matured, and decayed within a 10 h period between 1000 and 2000 UTC. At its peak around 1600 UTC, the MCS's areal extent of cold cloud top temperatures <208 K, a proxy for precipitating deep convective systems described in *Chen et al*. [1996], was comparable to that of *Tropical Storm 05A*, an active tropical cyclone centered near 15.0°N and 68.2°E in the Arabian Sea (Figure 1). The symmetry of the cloud shield, surrounded by a ring-shape moat featuring warmer cloud top temperatures, exemplified the special structure of this convective event, and its rapid development gave the visual impression of an "explosion."

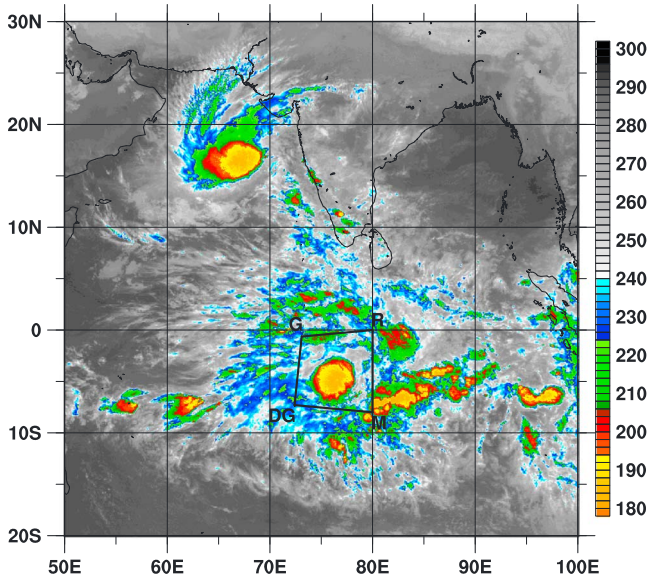

Figure 1. Meteosat-7 IR image of the Indian Ocean (IO) at 1600 UTC 28 November 2011. Color shading represents cloud top temperature (K) with red/yellow colors highlighting values <208 K, a proxy for precipitating deep convective systems described in *Chen et al.* [1996]. The DYNAMO southern sounding array is marked with the four launch sites at Gan Island (G), R/V *Revelle* (R), R/V *Mirai* (M), and Diego Garcia (DG).

2. Observations From DYNAMO

2.1. Integrated Sounding System

Four observation sites, including Gan Island ("G," Maldives, 0°S/73°E), Diego Garcia ("DG," British Indian Ocean Territory, 7°S/72°E) and the research vessels R/V *Revelle* ("R," 0°S/80°E) and R/V *Mirai* ("M," 8°S/80°E), encompassed the quadrilateral southern sounding array (Figure 1). The upper air observations were made with the integrated sounding system (ISS) [*Parsons et al.*, 1994; *Johnson and Ciesielski*, 2013]. Global Positioning System (GPS) radiosondes were launched from each of the ISS sites every 3 h, measuring the vertical profiles of temperature, pressure, humidity, and horizontal winds. These measurements are the first such ISS network observations obtained from the equatorial IO and provided an unprecedented data set for assessing the environmental conditions that fostered the explosive convective cloud system during the MJO initiation. Although the ISS sites were not in the immediate environment of this convective system, the continuous sounding data coverage provided valuable information on other MCSs upstream near the R/V *Revelle* and the synoptic-scale conditions that were evidently favorable for the development of organized convection.

2.2. Infrared and Microwave Satellite Data

In this study, we use Meteosat-7 infrared (IR, channel 8) satellite imagery to document the evolution of the convective cloud systems that occurred on 28 November 2011. The IR data have spatial and temporal resolutions of ~5 km and 30 min, respectively. Although multiple radars were available at Gan and on the research vessels, the location of the convective system in the middle of the DYNAMO array was out of the radar range. A National Oceanic and Atmospheric Administration (NOAA) P-3 research aircraft was stationed at Diego Garcia and used to investigate convective systems during MJO initiation in DYNAMO, but unfortunately, the aircraft was deployed outside of the DYNAMO array on 28 November. Thus, there were no in situ data from within the explosive MCS.

To represent MCSs using IR data, cloud clusters are identified as contiguous areas of IR brightness temperatures below a threshold value encompassing a contiguous area of at least 5000 km^2 (equivalent diameter of 80 km). The IR threshold value can be selected to identify certain convective properties. For example, 208 K is generally used for representing precipitating MCSs, based on results from previous studies over the western Pacific during the Tropical Ocean Global Atmosphere-Coupled Ocean-Atmosphere Response Experiment (TOGA COARE) [*Chen et al.*, 1996]. There is generally a close correspondence between the 208 K cloud area and contiguous mesoscale areas of rainfall observed by radar. In this study, we use the threshold value of 196 K to capture the main, intense convective features associated with the explosive convective system, highlighted in Figure 1 (yellow).

The 91 GHz channel ice-scattering data from the Special Sensor Microwave Imager/Sounder (SSMI/S) on board the Defense Meteorological Satellite Program's F-18 satellite are used to examine the characteristics of the convective system in terms of upper tropospheric ice content and the extent of the precipitating area. The SSMI/S instrument has a footprint resolution of 13.5 × 15.5 km^2.

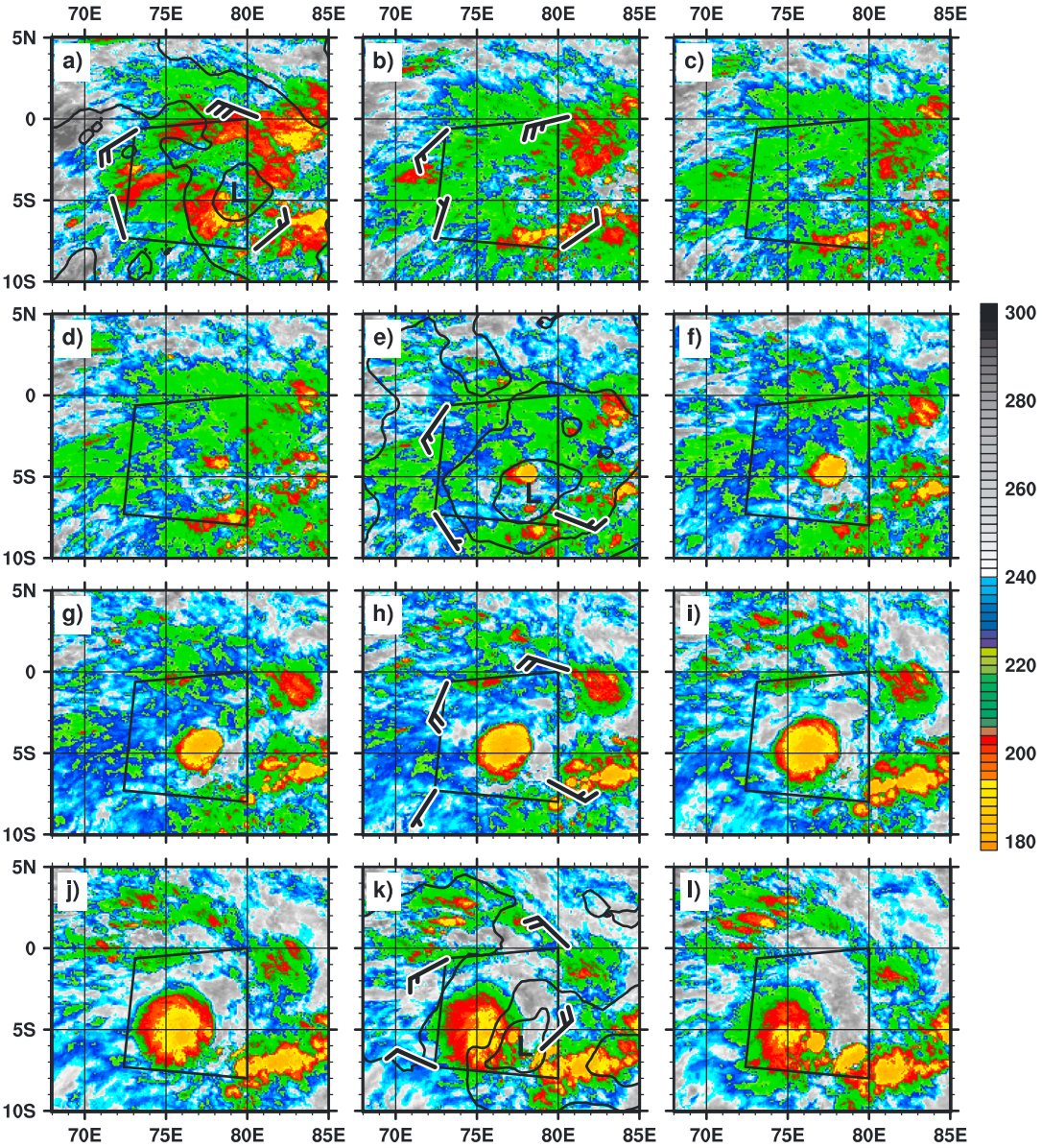

Figure 2. Same as for Figure 1, except for the central IO at (a) 0600 UTC, (b) 0900 UTC, (c) 1000 UTC, (d) 1100 UTC, (e) 1200 UTC, (f) 1300 UTC, (g) 1400 UTC, (h) 1500 UTC, (i) 1600 UTC, (j) 1700 UTC, (k) 1800 UTC, and (l) 1900 UTC 28 November 2011. Wind barbs in Figures 2a, 2b, 2e, 2h, and 2k represent the horizontal wind at the1000 hPa level based on radiosonde observations. The wind barbs are drawn following the meteorological convention with a full wind barb representing a wind speed of 5.0 m s^{-1}, while a half barb indicates 2.5 m s^{-1}. Black contours in Figures 2a, 2e, and 2k denote sea level pressure from 0600, 1200, and 1800 UTC ECMWF analyses (with contours of 1006, 1007, and 1008 hPa). "L" marks the center of the equatorial low-pressure system at the surface.

The area-averaged rain rate estimates from the Tropical Rainfall Measuring Mission (TRMM) 3B42V7 product have been used to quantify rainfall. The algorithm producing the data combines microwave and IR precipitations estimates, and the final gridded estimates have a 3 h temporal resolution and a 0.25° by 0.25° spatial resolution.

2.3. Satellite-Derived Upper Tropospheric Winds

Satellite-derived atmospheric motion vectors (AMVs), also known as cloud track winds, were used to examine the upper level wind conditions over the MJO initiation region. AMVs provide information about wind speed and direction at particular vertical levels and are calculated by an algorithm that tracks clouds in sequential geostationary satellite imagery [*Poteat*, 1973; *Sears and Velden*, 2012]. These vectors are

especially helpful in determining flow patterns in data sparse regions. However, AMVs are dependent on trackable clouds at a particular level of interest. Wind data in the upper troposphere are only available when sufficient cirrus clouds allow for the tracking algorithm to function.

2.4. ECMWF Model Analysis

To examine the mass field associated with the explosive convective system, we use the sea level pressure (SLP) from the European Centre for Medium-Range Weather Forecasts (ECMWF) model analysis fields. These fields were available at 6-hourly intervals with a 0.25° horizontal resolution. The SLP analyses allow for tracking the evolution of the equatorial low-pressure system.

3. Evolution of the Explosive MCS and Equatorial Low-Pressure System

3.1. Cloud Top Temperatures and Surface Observations

The rapid development of the explosive MCS and the concurrent evolution of the equatorial low-pressure system are shown in a series of Meteosat-7 IR images in Figure 2 from 0600 to 1900 UTC 28 November 2011. Throughout this study, times are given in UTC and can be converted to local standard time (LST) by adding 5 h. For reference, the panels in Figure 2 cover a time period from late morning (Figure 2a, 1100 LST) to midnight (Figure 2l, 0000 LST 29 November). The time difference between adjacent panels is 1 h, except for Figures 2a and 2b (top left), which are 3 h apart. The wind barbs in Figure 2 indicate the wind speed and direction at the 1000 hPa level (~80 m above sea level) based on sounding observations. Wind barbs are drawn following the meteorological convention, where each full barb corresponds to a wind speed of 5 m s^{-1} and a half barb to 2.5 m s^{-1}.

The main convective activity in the equatorial regions shown in Figures 1 and 2 was associated with the convective initiation of the MJO during DYNAMO. *Kerns and Chen* [2014] show that a significant portion of the convective activity was associated with westward moving synoptic-scale features that resemble Rossby- or mixed Rossby-gravity waves. The well-defined circulation detailed in this study can be characterized as a mixed Rossby-gravity wave-like system [*Kerns and Chen*, 2014, Figure 8]. At 0600 UTC (Figure 2a), the central equatorial IO was populated with numerous convective systems, where the coverage of precipitation was roughly equivalent to areas with cloud top temperatures $<$208 K (Figure 2, red and yellow colors). The near-surface wind at 0600 UTC was dominated by a well-defined low-level cyclonic circulation associated with the mixed Rossby-gravity wave-like system (clockwise flow as shown by the wind barbs in Figure 2a and in *Kerns and Chen* [2014, Figure 8]). Moderate to strong westerly winds (10–15 m s^{-1}) at Gan and the R/V *Revelle* as well as northeasterly flow at the R/V *Mirai* suggest that the center of circulation was located between those two latitude belts. Weaker winds prevailed at Diego Garcia, indicating a weaker pressure gradient in this area. The ECMWF SLP analysis from 0600 UTC (Figure 2a, black contours) agrees with the wind observations and clearly shows that the circulation was associated with an equatorial low-pressure system. *Kerns and Chen* [2014] showed that this low-pressure system was related to a westward propagating synoptic-scale feature similar to what has been described in *Wheeler and Kiladis* [1999], who attributed westward propagating disturbances in the MJO active phase to equatorial Rossby waves and mixed Rossby-gravity waves. The observed wind and pressure fields are consistent with the expected response to the atmospheric heating based on the idealized model by *Gill* [1980].

The convective activity over the DYNAMO region slowly decayed over the next few hours, as shown by the decreasing trend in cold cloud top temperatures in Figures 2b–2d. The decay in the afternoon hours was likely related to the diurnal oscillations with an afternoon minimum in cold cloud tops during the active phases of the MJO as shown in *Chen and Houze* [1997b]. In spite of the general weakening trend, the first signs of the explosive convective system can be seen around 1100 UTC, near 4°S and 79°E, where an area with cloud tops $<$200 K emerged (Figure 2d). The ECMWF SLP analysis from 1200 UTC indicates that the convective system developed close to the center of the low-pressure system, which had moved to the south-southwest (Figure 2e). It is likely that the circulation aided the development of the explosive MCS by providing favorable conditions, such as low-level convergence of moist and unstable air. The direction of the low-level winds at the R/V *Mirai* shows the flow directed toward the center of the low, which indicates convergence near the surface. The next couple of hours after 1200 UTC were characterized by the explosive

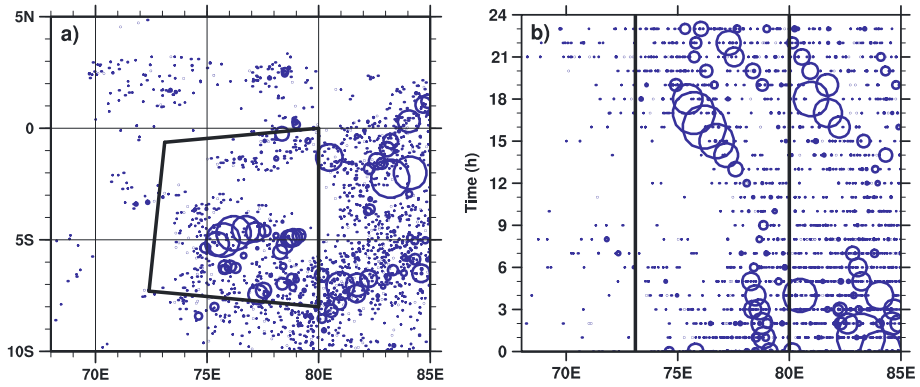

Figure 3. Cloud clusters with IR temperature <196 K from 0000 to 2300 UTC on 28 November 2011: (a) over the DYNAMO domain and (b) time-longitude diagram with cloud clusters within 10°S–5°N latitude band. The size of blue circles is proportional to the size of 196 K cloud clusters.

expansion of very cold cloud tops (Figures 2e–2i), and the system reached its peak around 1500–1600 UTC while becoming the single most prominent feature in the equatorial IO (Figures 2h and 2i). Note the remarkable pattern of a highly symmetric cloud shield with a diameter of ~470 km and the surrounding ring of much warmer cloud top temperatures (i.e., nonprecipitating clouds). At 1700 UTC, cloud top temperatures started to increase, a sign of weakening of the MCS (Figure 2j). As the system decayed, new MCSs continued to develop to the southeast, which indicates a favorable environment for deep convection in the general area (Figures 2k and 2l).

The evolution of the explosive convective system is best summarized by the cloud cluster map shown in Figure 3a, accompanied by a time-longitude diagram in Figure 3b. We use an IR temperature threshold of 196 K (−77°C) in this case, which is lower than the 208 K used for TOGA COARE in *Chen et al.* [1996], to highlight the large area of very cold cloud tops in this MCS. The explosive development of the convective system was preceded by another relatively large MCS to the east near 5°S and 79°E a few hours earlier, which dissipated at around 0600 UTC as shown in Figures 2a and 3b. The rapid development, explosive expansion in size of the 196 K cluster in the center of the DYNAMO array, and the westward propagation are well captured in Figure 3b.

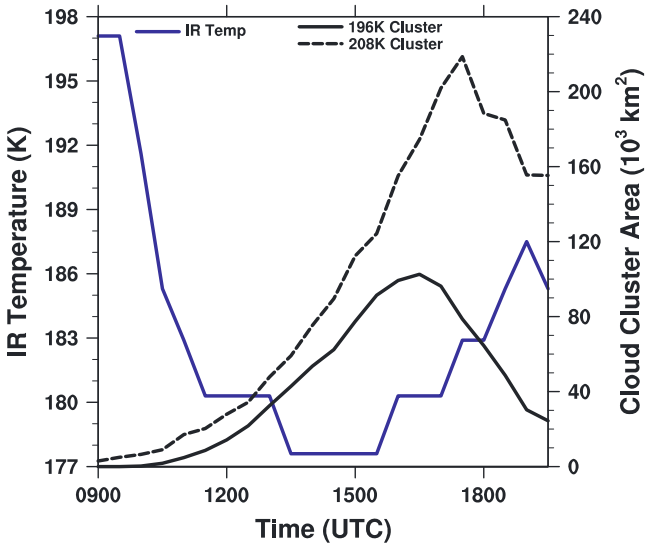

Figure 4. Time series of the minimum IR cloud top temperature (K), the areas of IR cloud top temperatures <196 K and 208 K (10^3 km^2), respectively, from 0900 to 1900 UTC on 28 November 2011.

To better quantify the evolution of the large MCS, Figure 4 shows time series of the minimum IR cloud top temperature, the areas of IR cloud top temperatures <196 K and 208 K, respectively, from 0900 to 1900 UTC on 28 November 2011. The coldest cloud top temperature dropped quickly from 197 K to ~177 K (−96°C) in 2–3 h, which is very cold even for equatorial deep convection. The rapid growth of the areas of the cold cloud tops, from 0 to 110,000 km^2 for 196 K and 3000 to 220,000 km^2 for 208 K, occurred between 1000 and 1700 UTC. The development of such a large explosive convective cloud system within the context of MJO initiation was only observed once during the 6 month DYNAMO Extended

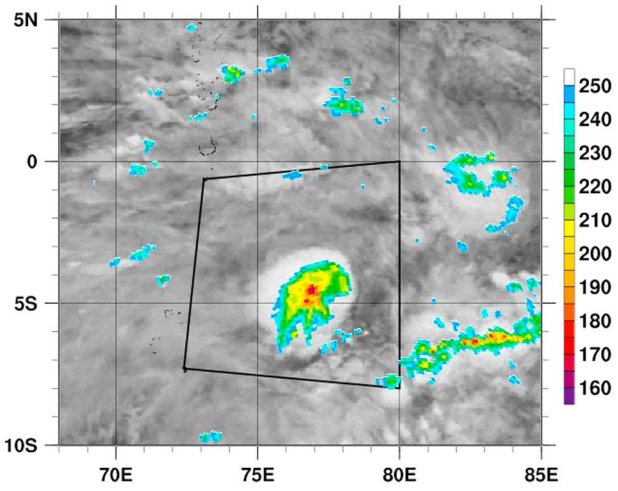

Figure 5. Meteosat-7 IR image from 1500 UTC 28 November 2011 (grey scale) overlaid with SSMI/S 91 GHz polarization corrected brightness temperature (PCT, color shading, K). The swath data from the SSMI/S instrument cover the period 1500–1505 UTC 28 November 2011.

Observing Period, which encompassed the development of three separate MJO initiation periods between October 2011 and March 2012.

A significant amount of ice lofted by deep convection is associated with the very cold cloud tops, as shown by the polarization corrected brightness temperature (PCT) from the SSMI/S instrument in Figure 5. The satellite pass occurred at 1500 UTC, around the time of maximum development of the explosive MCS. The SSMI/S data reveal that the coldest PCT in the 91 GHz band was 160 K, indicating large amount of ice in the upper troposphere. The SSMI/S data also allow for calculating the size of the contiguous area covered by precipitation, which can be regarded as a measure for the total mass flux associated with this convective system. The extent of the area encompassed by the 250 K PCT contour, a proxy for moderate and high rain rates of 3 mm h^{-1} or larger [*Mohr and Zipser*, 1996], was 80,817 km^2. This number illustrates that the system was unusually large for a single convective entity and among the largest classified by the statistical analysis in *Mohr and Zipser*'s [1996] study. According to their population statistics of convective systems, the MCS's extent of $>$80,000 km^2 made it fall into the upper 100th percentile bin in terms of size for IO systems. In fact, only ~5 out of 1097 convective systems observed in the IO during the course of their study were larger than the explosive MCS presented in this study, underlining the rarity of this event.

3.2. Vertical Velocities and Divergence Derived From DYNAMO Soundings

To put the event on 28 November in context of the entire 3 month DYNAMO intensive observational period, Figure 6 shows time series of DYNAMO sounding array-averaged vertical velocity, divergence, and relative vorticity fields derived from the ISS data from 1 October to 31 December 2011. This analysis highlights the coherent dynamic response to diabatic heating, which is a manifestation of forcing due to the convection. It is clear that the synoptic-scale low-pressure system and associated convective activity were the most significant event during DYNAMO as shown in the vertical velocity (Figure 6a, shading) and divergence (Figure 6a, contours) maxima on 28 November. The strength of the vertical velocity indicates vigorous upward motions and large vertical mass flux inside the array, which coincides with the rapid growth/expansion of cold cloud tops shown by the satellite IR data (Figures 2–4). A corresponding maximum in relative vorticity (negative values in Southern Hemisphere) and maximum in relative humidity occurred on 28 November (Figure 6b). The vorticity minimum associated with the low-pressure system is the most prominent feature over the entire 3 month period.

The vertically averaged heating rate derived from the sounding observations is shown in Figure 6c. It is mostly positive due to continued episodes of deep convection, and the most striking peak centered on 28 November with a heating rate close to 9 K d^{-1} is one of two largest daily values during the 3 month period. The TRMM area-averaged rain rate shows a corresponding maximum around the same time period (Figure 6d). Figure 6 (solid line) is the sounding array-averaged rain rate and the dashed line is the rain rate averaged within an area with radius of 1° centered on the R/V *Mirai* with an average rain rate of $>$120 mm d^{-1}.

Figure 7 zooms in on the time period from 0600 UTC 27 November to 1200 UTC 29 November 2011, and the stipples indicate the time during which the large MCS developed, matured, and decayed (1000–2000 UTC 28 November). Several interesting features are worth noting: (1) enhanced low-level convergence was observed on 27 November (Figure 7a), a day before the development of the large MCS, (2) the strongest array-averaged

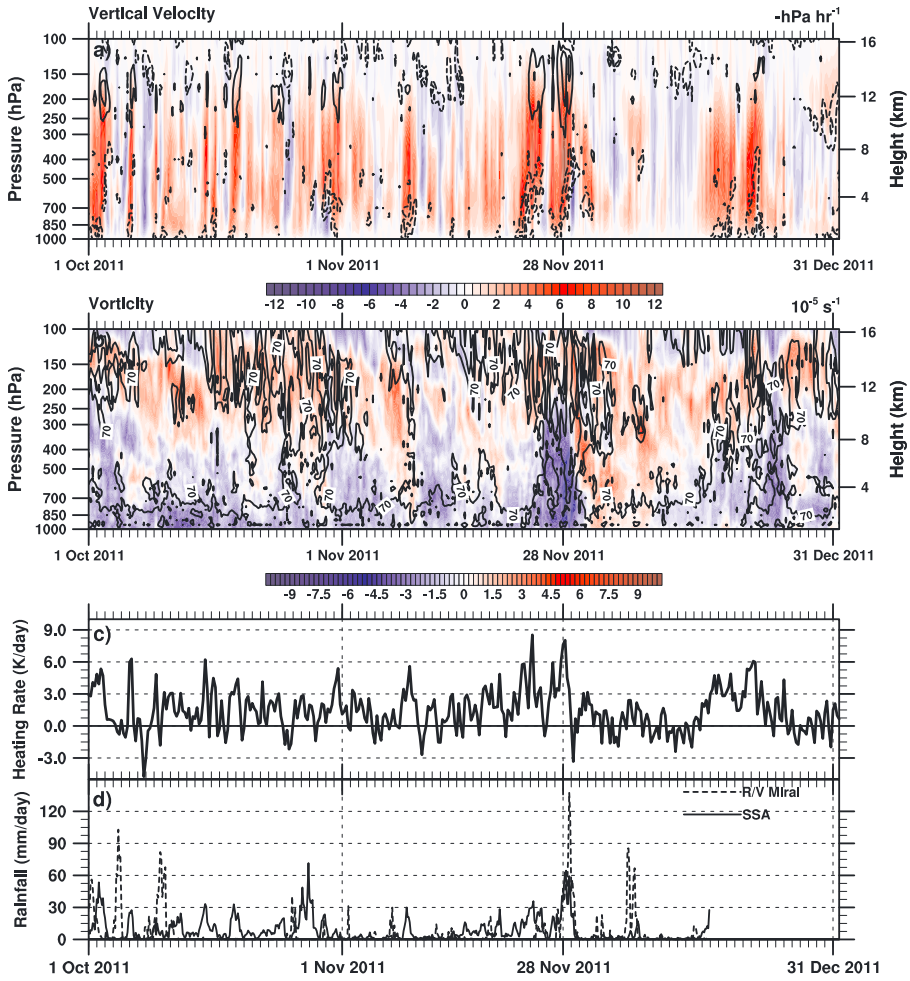

Figure 6. Time series from 1 October to 31 December 2011: (a) sounding array averaged vertical velocity (shading, hPa h^{-1}) and divergence (dashed: −10, −5; solid: 10, 20 contours in 10^{-6} s^{-1}), (b) relative vorticity (shading, 10^{-5} s^{-1}) and relative humidity (black contours, 70% and 90%), (c) vertically averaged heating rate (K d^{-1}), and (d) TRMM 3b42V7 rain rate estimates (mm d^{-1}, solid line: sounding array average, dashed line: average over a circular area with 1° radius centered on the R/V *Mirai*) .

vertical velocities appeared at ~0600 UTC (Figure 7a), perhaps an indication of strong convection, shortly before the rapid expansion of the cold cloud tops of the MCS from 1000 to 1700 UTC (Figure 4), and (3) a short-lived vorticity maximum (Figure 7b) was observed shortly after the MCS reached its maximum areal extent at 1800 UTC (Figure 4), suggesting a strengthened cyclonic circulation.

In summary, the rapid development of the large MCS was preceded by the enhanced low-level convergence associated with the equatorial low-pressure system. The large MCS helped strengthen the synoptic cyclonic circulation within the large-scale MJO convective envelope. These observations show a complex multiscale interaction in MJO initiation over the IO.

4. Environmental Winds and Thermodynamic Profiles

4.1. Upper Tropospheric Winds

Figure 8 displays the upper tropospheric winds over the tropical IO at 0500, 0900, and 1600 UTC 28 November 2011. Satellite-derived wind vectors from above the 250 hPa level (>10.5 km altitude) are included. Regions of active convection are outlined in Figure 8 (black contours), which correspond to cloud top temperatures <208 K. Figure 8 shows that the upper level flow was generally dominated by easterlies. South of the equator and over the DYNAMO region, the flow featured a northerly component. At 0500 UTC (Figure 8a), strong upper level northeasterly winds prevailed just west of the active convections with some wind barbs

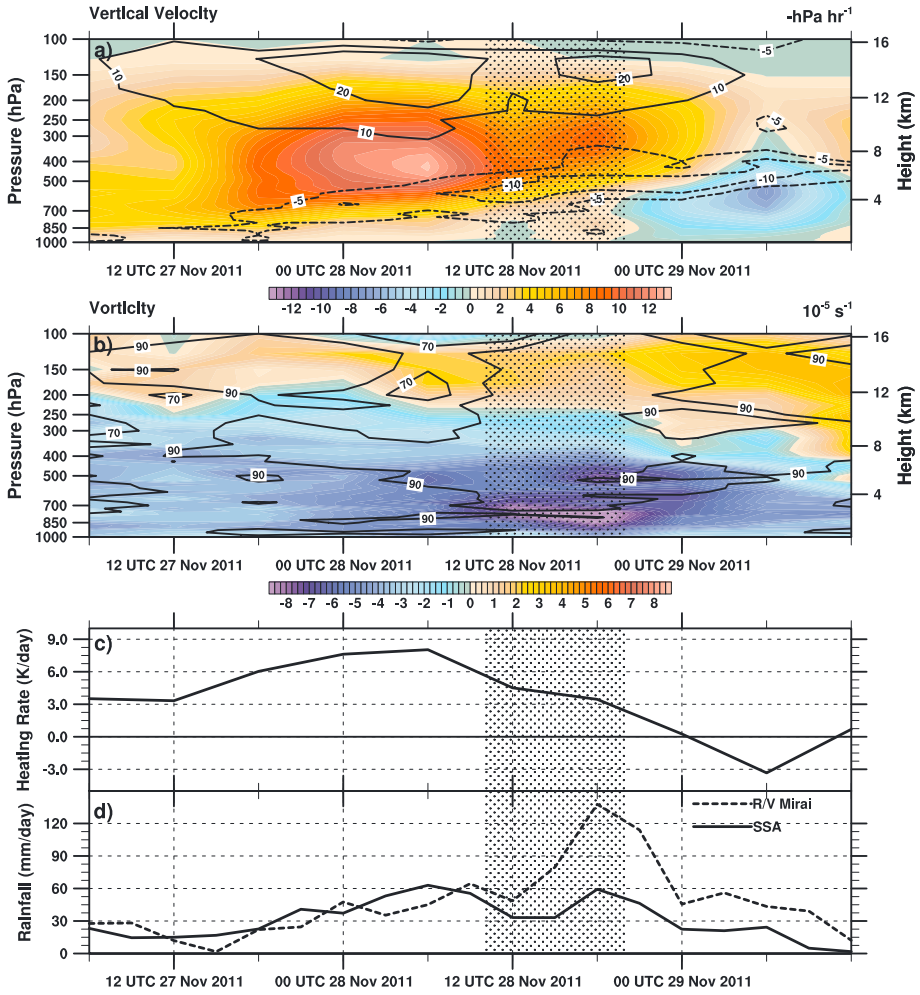

Figure 7. Same as in Figure 6, except for time period from 0600 UTC 27 November to 1200 UTC 29 November 2011. Stippled column indicates the time period when the explosive expansion of cold cloud tops of the MCS occurred shown in Figure 4.

indicating a speed of $>30\ m\ s^{-1}$ over the DYNAMO array. In the regions with heavy convective activity near the equator, upper tropospheric wind speeds were generally below $20\ m\ s^{-1}$. Slightly east of the vigorous convection on the equator, the upper level wind speed was significantly reduced ($<10\ m\ s^{-1}$, 85–90°E). We suspect that the reduction in upper level easterlies is a manifestation of the superposition of the environmental easterly winds and the convective outflow in the region. A few hours later at 0900 UTC (Figure 8b), some convection within the DYNAMO array and near its northeastern corner had dissipated. The upper level winds within the DYNAMO array had weakened compared to 4 h earlier (Figures 8a and 8b). Furthermore, an area of upper level divergence is evident in Figure 8b. The wind vectors over the DYNAMO region indicate that the flow was uniformly directed from northeast to southwest and featured a pronounced difference in speed. In the southwestern DYNAMO array and adjacent areas, the prevailing upper level winds had a speed of $25–30\ m\ s^{-1}$, whereas in the northeastern regions the wind speed was generally around $20\ m\ s^{-1}$ or less. The upper level divergence is consistent with the synoptic-scale ascent over the DYNAMO array shown in Figures 6a and 7a. The upper level winds have been further reduced at 1600 UTC, when the explosive MCS reached peak areal extent of cloud top temperature <208 K (Figure 8c).

4.2. Evolution of Wind Profiles in the DYNAMO Array

While the cloud track winds in Figure 8 allow for analyzing the flow in the upper levels where cirrus clouds were present, the middle and lower tropospheric levels were hidden from the satellite view because of the extensive upper level cloud layer on 28 November. Vertical wind profiles from the DYNAMO ISS data offer the

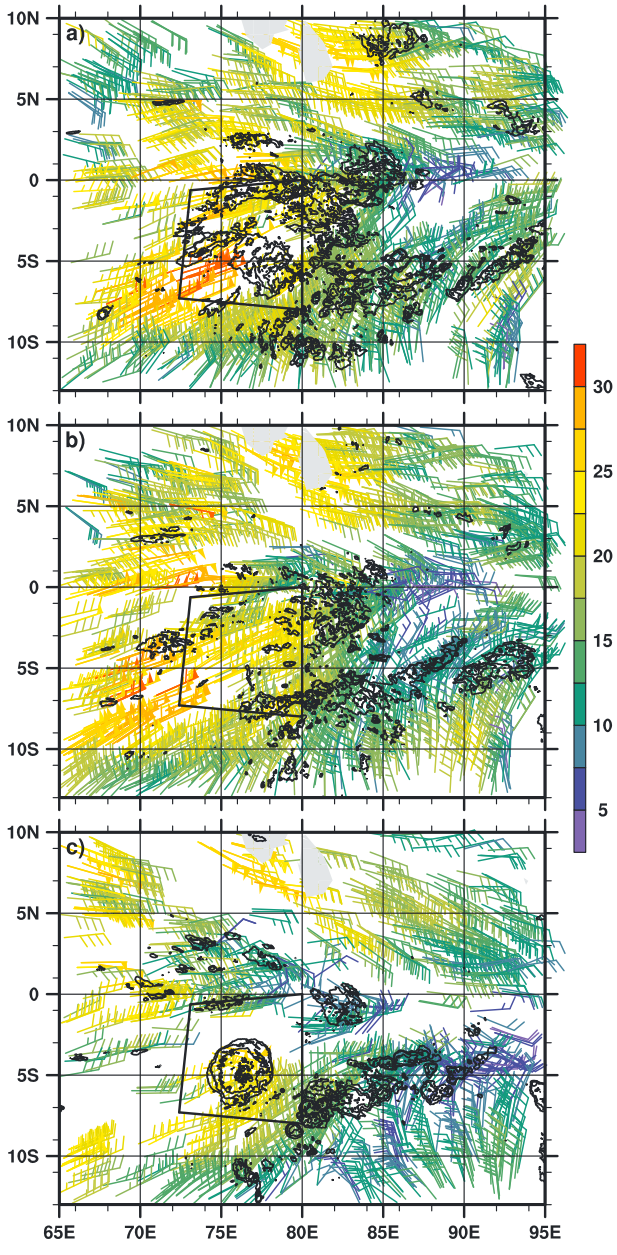

Figure 8. Satellite-derived atmospheric motion vectors (AMVs) above the 250 hPa level at (a) 0500 UTC, (b) 0900 UTC, and (c) 1600 UTC 28 November 2011 over the tropical Indian Ocean. Wind speed is color-coded (m s^{-1}). Black contours denote cloud top temperatures $<$208 K from Meteosat-7 IR data.

opportunity to analyze the evolution of the winds throughout the entire troposphere, regardless of meteorological conditions and at a much higher vertical resolution and accuracy. Figure 9 displays the vertical profiles of the horizontal wind for a 24 h period from 0000 UTC 28 to 29 November 2011 at the four sounding sites. Each panel shows a time series of wind data gathered by the radiosondes that were launched in 3-hourly intervals.

The time series of sounding wind data at Gan (Figure 9a) shows little temporal variability throughout the 24 h period and exhibits the typical zonal flow pattern prevailing west of the MJO convective center. Vigorous upper level easterlies and low-level westerlies created strong vertical wind shear. The prevailing flow at the R/V *Revelle* was more complex and variable with time (Figure 9b, no radiosonde was launched from the R/V *Revelle* at 1200 UTC). The upper level easterlies were weaker during the period of active convection near the *Revelle* between 0000 and 0900 UTC and increased to $>$30 m s^{-1} after 1800 UTC. The lower levels were dominated by westerly winds associated with the equatorial low-pressure system. In comparison with the Gan wind profiles, the vertical wind shear at the R/V *Revelle* was significantly less during the period of active convection due to the lack of strong upper level easterly flow from 12 to 16 km (Figures 9a and 9b, 0000–1500 UTC). The reduced vertical wind shear over a deep layer may be a result of combination of convective outflow and vertical momentum transport/mixing by deep convection near the R/V *Revelle*, upstream of the explosive MCS. A pronounced upper level jet appeared after the convective activity waned near the R/V *Revelle* and the environmental upper tropospheric easterlies protruded into the region. Compared to the equatorial sites Gan and R/V *Revelle*, the off-equator sites Diego Garcia (Figure 9c) and R/V *Mirai* (Figure 9d) featured easterly flow at all levels above 3–4 km. The turning of the low-level winds at the R/V *Mirai* late on 28 November (Figure 9d) was associated with the low-pressure systems moving south-southwestward through the array. The quick transition from easterly to westerly occurred as the low's surface center passed very close to the ship (Figure 9d, 1500–0000 UTC and Figures 2h and 2k). Considering the R/V *Mirai*'s proximity slightly upstream of the explosive convective event, the vertical wind profile at this location is likely best approximating the flow near the explosion. In contrast to the western two locations shown in Figures 9a and 9c, the wind profile at the R/V *Mirai* indicates significantly

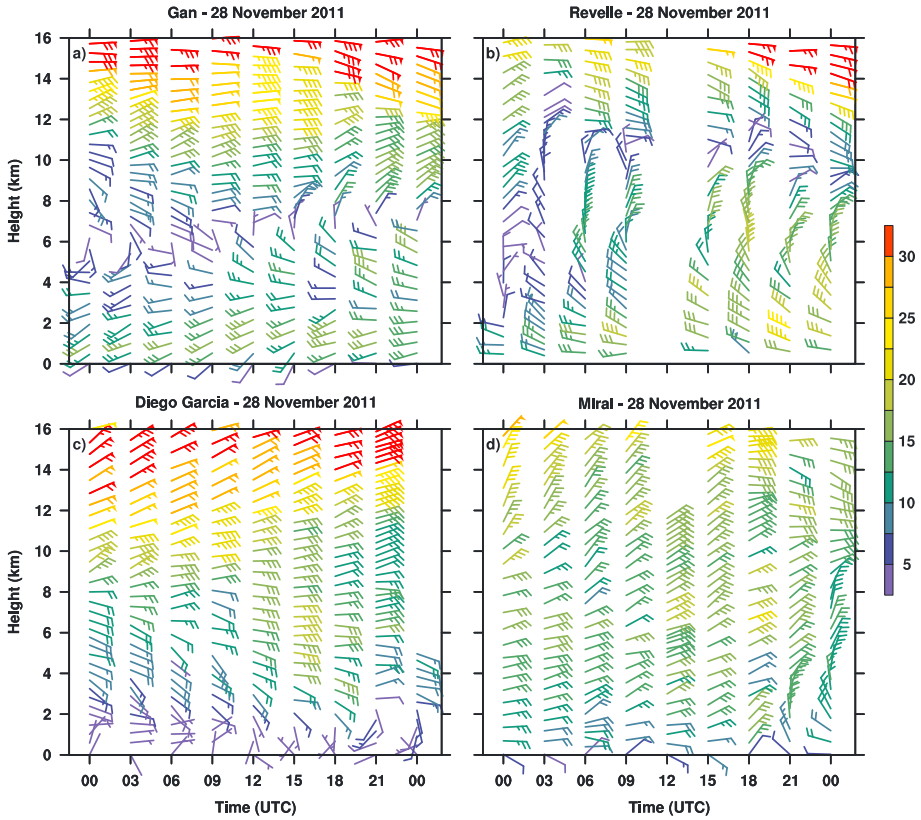

Figure 9. Time series of 3-hourly vertical profiles of the horizontal wind at (a) Gan, (b) R/V *Revelle*, (c) Diego Garcia, and (d) R/V *Mirai* on 28 November 2011. The radiosonde data were not available at the *Revelle* and partly missing at the *Mirai* at 1200 UTC. Wind barbs and color shading represent the direction and wind speed (m s^{-1}), respectively.

reduced shear, similar to what was observed at the R/V *Revelle* during the period when the ship was near multiple large convective systems (Figure 9b, 0000–0900 UTC).

In general, a common trend in the four wind profile time series seems to be the reduction of vertical wind shear during convectively active periods due to significantly weaker upper level easterly flow. The lack of strong shear is especially pronounced near the R/V *Mirai*, which was closest to the explosive MCS.

4.3. Thermodynamic Conditions

Deep, moist convection, and organized MCS in particular can only develop when certain atmospheric conditions are met. *Johns and Doswell* [1992] popularized an ingredient-based approach to atmospheric deep moist convection. They stated that deep moist convection only occurs when (1) a sufficiently large moist layer, (2) moist conditional instability, and (3) a source of lift are present. An analysis of moisture and instability derived from radiosonde observations will be presented and its role in the development and intensity of the explosive MCS assessed.

The soundings from the DYNAMO array offer a detailed look at the vertical profiles of temperature and moisture during the development of the explosive MCS (Figure 10). Convective available potential energy (CAPE), a quantity representing moist conditional instability, and total precipitable water (TPW), a measure of the integrated atmospheric water vapor content, were calculated from the sounding observations. The amount of CAPE is an approximation for the maximum potential intensity of updrafts. However, a direct conversion of CAPE to updraft velocity is more complex since it involves assumptions about the effects of liquid water load on a rising air parcel, vertical pressure forces, and entrainment processes. If all the CAPE were converted to kinetic energy, the vertical velocity of an air parcel would reach $w_{CAPE} = [2(CAPE)]^{0.5}$ at the equilibrium level. A simple approximation to account for the aforementioned factors reducing the vertical velocity of an updraft is to assume a 50% efficiency for the conversion of CAPE into vertical kinetic energy

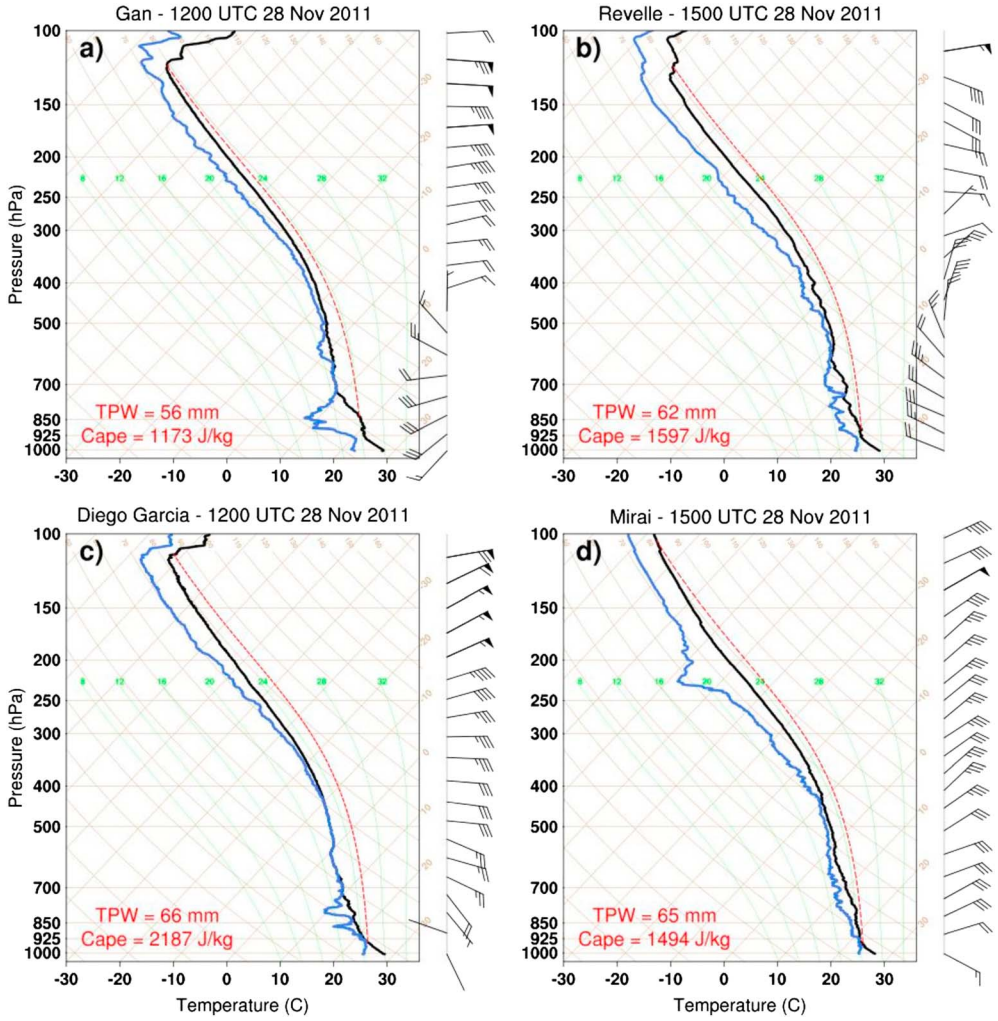

Figure 10. Radiosonde observations from (a) Gan at 1200 UTC, (b) R/V *Revelle* at 1500 UTC, (c) Diego Garcia at 1200 UTC, and (d) R/V *Mirai* at 1500 UTC 28 November 2011. Temperature profiles are black, dew point profiles blue, and the dashed red line denotes a hypothetical curve of an air parcel rising from the surface. Total precipitable water (TPW) and convective available potential energy (CAPE) values are derived from the soundings.

[*Zipser*, 2003]. In this case the maximum vertical velocity can be calculated according to $w_{\mathrm{CAPE}}^{\mathrm{eff}} = (\mathrm{CAPE})^{0.5}$. However, the resulting $w_{\mathrm{CAPE}}^{\mathrm{eff}}$ of 39 m s^{-1} is much larger than what has been reported in the literature. According to aircraft observations, a more realistic value for the maximum updraft velocity associated with an ambient CAPE value of 1500 J kg^{-1} over the tropical ocean would be around 17 m s^{-1} [*LeMone and Zipser*, 1980; *Jorgensen and LeMone*, 1989].

The sounding data in Figure 10 are plotted in conventional Skew-T/Log-P diagram form. Temperature and dew point curves are black and blue, respectively, and the red lines denote the lifting curve of a hypothetical air parcel lifted from the surface without entrainment. The area between the red and black curve is proportional to the CAPE. The data displayed in Figure 10 are from the 1200 UTC radiosonde launches at Gan (Figure 10a) and Diego Garcia (Figure 10c), and from the 1500 UTC launches at the research vessels (Figures 10b and 10d). All four soundings show high amounts of atmospheric moisture, and the TPW content exceeded 60 mm at the R/V *Revelle* (Figure 10b), R/V *Mirai* (Figure 10d), and Diego Garcia (Figure 10c). The sounding from Gan (Figure 10a) features a somewhat lower TPW value and exhibits a pronounced dry layer below 700 hPa, related to a dry air intrusion described in *Kerns and Chen* [2014]. Note that the Skew-T diagram of the *R/V Mirai* sounding (Figure 10d) does not show the tropopause, whereas it is depicted in the other 3 soundings between 125 and 100 hPa. This hints at the remarkable depth of the troposphere, which was deeper

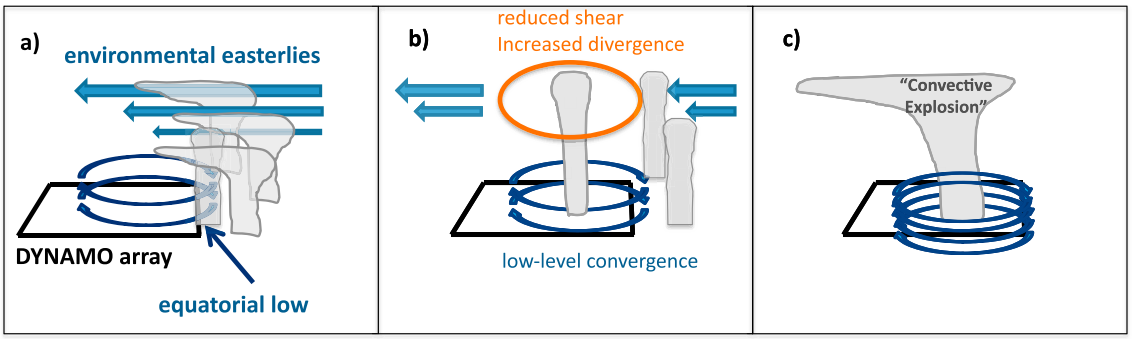

Figure 11. Schematic of the explosive convective event observed on 28 November 2011 during DYNAMO over the equatorial Indian Ocean: (a) predevelopment, (b) early development, and (c) mature stages. The black rectangle marks the DYNAMO array with the corner points at Diego Garcia, Gan, R/V *Revelle*, and R/V *Mirai* as shown in Figure 1. Circular arrows indicate the low-level flow associated with the equatorial low (mixed Rossby-gravity wave-like system) and straight arrows show the upper level environmental easterly winds.

than 16 km at this location (the 100 hPa level corresponds to 16 km altitude). The CAPE values in all soundings exceed 1000 J kg^{-1}, indicating ample conditional instability. These values are in agreement with previous studies, which found CAPE values of 1500 J kg^{-1} representative of the environment near tropical oceanic MCSs.

We can summarize this section by stating that the soundings indicate that all necessary conditions for the occurrence of vigorous deep convection were met on 28 November 2011. The troposphere in the DYNAMO region near the explosive MCS was very moist, conditionally unstable, and the low-level circulation supplied a broad area of lift by convergence in the boundary layer.

5. Summary and Conclusions

The rapid development of a large, explosive convective cloud system on 28 November 2011 provided a unique opportunity to examine the interactions between organized convection and the large-scale environment in MJO initiation during DYNAMO. The areal extent of cold cloud tops (Figures 2–4) and ice content (Figure 5) make this MCS a top-ranked system based on the statistics of IO convective system population. Sounding observations from the DYNAMO array and ECMWF SLP analyses indicate that a vigorous synoptic-scale equatorial low-pressure system dominated the lower-level flow within the DYNAMO array on 28 November. The large magnitude of array-averaged low-level convergence, vertical velocity, and a pronounced maximum in relative vorticity derived from the sounding data show a strong low-level forcing where the MCS developed (Figures 6 and 7).

The large-scale flow in the equatorial regions was dominated by low-level westerlies and strong upper level easterlies (above ~10 km), indicating a highly sheared large-scale environment. However, the regions near and upstream of the explosive MCS featured significantly less wind shear (Figure 9). Upper tropospheric wind analyses show that the strong zonal flow in the upper troposphere weakened before the initiation of the explosive convective event (Figure 8). We suspect that multiple MCSs associated with a mixed Rossby-gravity wave-like system observed during the active phase of the MJO [*Kerns and Chen*, 2014] may have reduced the strong upper level easterlies through convective outflow and vertical momentum transfer.

The evolution of the explosive MCS and its large-scale environment can be summarized in a schematic shown in Figure 11. Prior to the development of the large MCS, multiple convective systems were active upstream of the DYNAMO array where the upper level winds are predominantly strong easterlies with relatively high vertical wind shear (Figure 11a). The convective outflow and vertical momentum transport by the deep convection modulated the environmental flow by reducing the strong upper level easterlies downstream of the convection. The cyclonic circulation associated with the low-pressure system reduced the equatorial westerlies. Both factors lead to a reduction in vertical wind shear over the DYNAMO array (Figure 11b). Enhanced low-level convergence and upper level divergence associated with the equatorial low-pressure system created favorable conditions for the development of the explosive MCS, which in turn strengthened the low-level cyclonic circulation at the end (Figure 11c).

The near-circular cold cloud shield of the MCS presented in this study (Figure 2) suggests that this convective system was not a canonical squall line-type MCS that is typically observed in a strong low-level shear

environment as suggested by *Rotunno et al.* [1988]. The shear needs to be strong enough to balance the circulation generated by the squall line's cold pools in order to sustain the convective line. Observations of tropical squall lines [e.g., *Zipser*, 1977; *LeMone et al.*, 1998] showed that the convective lines are usually oriented perpendicular to the low-level to midlevel shear. In fact, the lack of distinct line-type MCSs was a recurring observation on many of the NOAA P-3 research flights during DYNAMO. Jorgensen (personal communication, 2011) noted that the structure of convective systems over the IO seems to be more nonsquall line-type than compared to what had been observed during earlier field experiments in the tropics, such as Global Atmospheric Research Program Atlantic Experiment and TOGA COARE. It is an open question whether convective organization is different during MJO initiation than in other large-scale environments.

In conclusion, in situ sounding observations from DYNAMO provided a rare opportunity for us to examine the intricate relationship among an equatorial low-pressure system, an explosive convective cloud system observed by satellite, and the large-scale equatorial flow during the MJO initiation over the Indian Ocean. The results from this study suggest that there were two key contributors to the explosive development of the large MCS on 28 November. First, synoptic-scale forcing associated with the low-pressure system provided strong low-level convergence over the DYNAMO sounding array leading up to the development of the large MCS. Second, widespread deep convection (that may have been forced by the same low-pressure system) upstream of the MCS played an important role in reducing vertical wind shear associated with the MJO zonal flow, which paved the way for more organized convective systems. A significant portion of the convective activity during MJO initiation was associated with Rossby- or mixed Rossby-gravity wave-like synoptic-scale systems during DYNAMO as shown in *Kerns and Chen* [2014]. Furthermore, the large MCS in turn further strengthened the synoptic-scale cyclonic circulation. These types of multiscale convection-environment interactions may be a key to better understand and predict MJO initiation over the equatorial Indian Ocean. Our findings agree with current modeling studies such as *Holloway et al.* [2013], which also indicate that a realistic representation of convection-environment feedback processes is crucial to skillfully predicting the MJO with state-of-the-art numerical weather prediction models.

A final remark on the fate of the equatorial low-pressure system that was intimately linked to the explosive MCS, it continued on its southwestward path after 28 November 2011 and produced sporadic bursts of deep convection along the way. Meteo-France upgraded the system to tropical depression status on 6 December 2011 when it was located about 800 km south-southwest of Diego Garcia. The system remained a weak tropical cyclone, and finally dissipated on 16 December over the southern IO, more than 2 weeks after it had formed during the MJO initiation [*Kerns and Chen*, 2014] and interacted with the explosive MCS over the DYNAMO sounding array on 28 November.

Acknowledgments

We thank Brandon Kerns for his assistance during the course of this study. The AMV data were provided by the Cooperative Institute for Meteorological Satellite Studies (CIMSS)/University of Wisconsin and the DYNAMO sounding data by Richard Johnson and Paul Ciesielski of the Colorado State University. Ed Zipser and two anonymous reviewers provided constructive comments and suggestions that helped improve the manuscript. This research is supported by research grants from NSF (AGS1062242), NOAA (NA11OAR4310077), and ONR (N000141110562).

References

Benedict, J., and D. A. Randall (2009), Structure of the Madden-Julian Oscillation in the superparameterized CAM, *J. Atmos. Sci.*, *66*, 3277–3296, doi:10.1175/2009JAS3030.1.

Biello, J. A., and A. J. Majda (2005), A new multiscale model for the Madden–Julian Oscillation, *J. Atmos. Sci.*, *62*, 1694–1721, doi:10.1175/JAS3455.1.

Chen, S. S., and R. A. Houze Jr. (1997a), Interannual variability of deep convection over the tropical warm pool, *J. Geophys. Res.*, *102*, 25,783–25,795, doi:10.1029/97JD02238.

Chen, S. S., and R. A. Houze Jr. (1997b), Diurnal variation and life-cycle of deep convective systems over the tropical pacific warm pool, *Q. J. R. Meteorol. Soc.*, *123*, 357–388, doi:10.1175/1520-0469(1996)053<1380:MVODCI>2.0.CO;2.

Chen, S. S., R. A. Houze Jr., and B. E. Mapes (1996), Multiscale variability of deep convection in relation to large-scale circulation in TOGA COARE, *J. Atmos. Sci.*, *53*, 1380–1409, doi:10.1175/1520-0469(1996)053<1380:MVODCI>2.0.CO;2.

Dunkerton, T. J., and F. X. Crum (1995), Eastward propagating ~2- to 15-day equatorial convection and its relation to the tropical intraseasonal oscillation, *J. Geophys. Res.*, *100*, 25,781–25,790, doi:10.1029/95JD02678.

Gill, A. E. (1980), Some simple solutions for heat-induced tropical circulation, *Q. J. R. Meteorol. Soc.*, *106*, 447–462, doi:10.1002/qj.49710644905.

Holloway, C. E., S. J. Woolnough, and G. M. S. Lister (2013), The effects of explicit versus parameterized convection on the MJO in a large-domain high-resolution tropical case study. Part I: Characterization of large-scale organization and propagation, *J. Atmos. Sci.*, *70*, 1342–1369, doi:10.1175/JAS-D-12-0227.1.

Houze, R. A., Jr. (1977), Structure and dynamics of a tropical squall-line system, *Mon. Weather Rev.*, *105*, 1540–1567, doi:10.1175/1520-0493(1977)105<1540:SADOAT>2.0.CO;2.

Houze, R. A., Jr., S. S. Chen, E. Kingsmill, Y. Serra, and S. E. Yuter (2000), Convection over the Pacific warm pool in relation to the atmospheric Kelvin-Rossby wave, *J. Atmos. Sci.*, *57*, 3058–3089, doi:10.1175/1520-0469(2000)057<3058:COTPWP>2.0.CO;2.

Johns, R. H., and C. A. Doswell (1992), Severe local storms forecasting, *Weather Forecast.*, *7*, 588–612, doi:10.1175/1520-0434(1992)007<0588:SLSF>2.0.CO;2.

Johnson, R. H., and P. E. Ciesielski (2013), Structure and properties of Madden-Julian Oscillations deduced from DYNAMO sounding arrays, *J. Atmos. Sci.*, *70*, 3157–3179, doi:10.1175/JAS-D-13-065.1.

Jorgensen, D. P., and M. A. LeMone (1989), Vertical velocity characteristics of oceanic convection, *J. Atmos. Sci.*, *46*, 621–640, doi:10.1175/1520-0469(1989)046<0621:VVCOOC>2.0.CO;2.
Kerns, B. W., and S. S. Chen (2014), Equatorial dry air intrusion and related synoptic variability in MJO initiation during DYNAMO, *Mon. Weather Rev.*, *142*, 1326–1343, doi:10.1175/MWR-D-13-00159.1.
LeMone, M. A., and E. J. Zipser (1980), Cumulonimbus vertical velocity events in GATE. Part I: Diameter, intensity and mass flux, *J. Atmos. Sci.*, *37*, 2444–2457, doi:10.1175/1520-0469(1980)037<2444:CVVEIG>2.0.CO;2.
LeMone, M. A., G. M. Barnes, and E. J. Zipser (1984), Momentum flux by lines of cumulonimbus over the tropical oceans, *J. Atmos. Sci.*, *41*, 1914–1932, doi:10.1175/1520-0469(1984)041<1914:MFBLOC>2.0.CO;2.
LeMone, M. A., E. J. Zipser, and S. B. Trier (1998), The role of environmental shear and thermodynamic conditions in determining the structure and evolution of mesoscale convective systems during TOGA COARE, *J. Atmos. Sci.*, *55*, 3493–3518, doi:10.1175/1520-0469(1998)055<3493:TROESA>2.0.CO;2.
Lin, J.-L., et al. (2006), Tropical intraseasonal variability in 14 IPCC AR4 climate models. Part I: Convective signals, *J. Clim.*, *19*, 2665–2690, doi:10.1175/JCLI3735.1.
Lin, H., G. Brunet, and J. Derome (2008), Forecast skill of the Madden–Julian Oscillation in two Canadian atmospheric models, *Mon. Weather Rev.*, *136*, 4130–4149, doi:10.1175/2008MWR2459.1.
Madden, R. A., and P. R. Julian (1971), Detection of a 40-50 day oscillation in the zonal wind in the tropical Pacific, *J. Atmos. Sci.*, *28*, 702–708, doi:10.1175/1520-0469(1971)028<0702:DOADOI>2.0.CO;2.
Madden, R. A., and P. R. Julian (1972), Description of global-scale circulation cells in the tropics with a 40–50 day period, *J. Atmos. Sci.*, *29*, 1109–1123, doi:10.1175/1520-0469(1972)029<1109:DOGSCC>2.0.CO;2.
Matthews, A. J. (2008), Primary and successive events in the Madden–Julian Oscillation, *Q. J. R. Meteorol. Soc.*, *134*, 439–453, doi:10.1002/qj.224.
Mechem, D. B., S. S. Chen, and R. A. Houze Jr. (2006), Momentum transport processes in the stratiform regions of mesoscale convective systems over the western Pacific warm pool, *Q. J. R. Meteorol. Soc.*, *132*, 709–736, doi:10.1256/qj.04.141.
Mohr, K. I., and E. J. Zipser (1996), Defining mesoscale convective systems by their 85-GHz ice-scattering signatures, *Bull. Am. Meteorol. Soc.*, *77*, 1179–1189, doi:10.1175/1520-0493(1996)124<2417:MCSDBT>2.0.CO;2.
Moncrieff, M. W. (2004), Analytic representation of the large-scale organization of tropical convection, *J. Atmos. Sci.*, *61*, 1521–1538, doi:10.1175/1520-0469(2004)061<1521:AROTLO>2.0.CO;2.
Nasuno, T. (2013), Forecast skill of Madden-Julian Oscillation events in a global nonhydrostatic model during the CINDY2011/DYNAMO observation period, *SOLA*, *19*, 69–73, doi:10.2151/sola.2013-016.
Parsons, D., et al. (1994), The integrated sounding system: Description and preliminary observations from TOGA COARE, *Bull. Am. Meteorol. Soc.*, *75*, 553–567, doi:10.1175/1520-0477(1994)075<0553:TISSDA>2.0.CO;2.
Poteat, K. O. (1973), A comparison of satellite-derived, low-level and cirrus-level winds with conventional wind observations, *J. Appl. Meteorol.*, *12*, 1416–1419, doi:10.1175/1520-0450(1973)012<1417:ACOSDL>2.0.CO;2.
Rotunno, R., J. B. Klemp, and M. L. Weisman (1988), A theory for strong, long-lived squall lines. *J. Atmos. Sci.*, *45*, 463–485, doi:10.1175/1520-0469(1988)045<0463:ATFSLL>2.0.CO;2.
Sears, J., and C. S. Velden (2012), Validation of satellite-derived atmospheric motion vectors and analyses around tropical disturbances, *J. Appl. Meteorol. Climatol.*, *51*, 1823–1834, doi:10.1175/JAMC-D-12-024.1.
Seo, K. H., W. Q. Wang, J. Gottschalck, Q. Zhang, J. K. E. Schemm, W. R. Higgins, and A. Kumar (2009), Evaluation of MJO forecast skill from several statistical and dynamical forecast models, *J. Clim.*, *22*, 2372–2388, doi:10.1175/2008JCLI2421.1.
Wheeler, M., and G. N. Kiladis (1999), Convectively coupled equatorial waves: Analysis of clouds and temperature in the wavenumber–frequency domain, *J. Atmos. Sci.*, *56*, 374–399, doi:10.1175/15200469(1999)056<0374:CCEWAO>2.0.CO;2.
Yamada, H., K. Yoneyama, M. Katsumata, and R. Shirooka (2010), Observations of a super cloud cluster accompanied by synoptic-scale eastward-propagating precipitating systems over the Indian Ocean, *J. Atmos. Sci.*, *67*, 1456–1473, doi:10.1175/2009JAS3151.1.
Yang, D. (2011), Testing the hypothesis that the MJO is a mixed Rossby–gravity wave packet, *J. Atmos. Sci.*, *68*, 226–239, doi:10.1175/2010JAS3563.1.
Yoneyama, K., C. Zhang, and C. N. Long (2013), Tracking pulses of the Madden-Julian Oscillation, *Bull. Am. Meteorol. Soc.*, *94*, 1871–1891, doi:10.1175/BAMS-D-12-00157.1.
Zhang, C. (2005), Madden-Julian Oscillation, *Rev. Geophys.*, *43*, RG2003, doi:10.1029/2004RG000158.
Zhang, C., M. Dong, S. Gualdi, H. H. Hendon, E. D. Maloney, A. Marshall, K. R. Sperber, and W. Wang (2006), Simulations of the Madden-Julian Oscillation in four pairs of coupled and uncoupled global models, *Clim. Dyn.*, *27*, 573–592, doi:10.1007/s00382-006-0148-2.
Zipser, E. J. (1977), Mesoscale and convective–scale downdrafts as distinct components of squall-line structures, *Mon. Weather Rev.*, *105*, 1568–1589, doi:10.1175/1520-0493(1977)105<1568:MACDAD>2.0.CO;2.
Zipser, E. J. (2003), Some views on "Hot Towers" after 50 years of tropical field programs and two years of TRMM data, *Meteorol. Monogr.*, *29*, 49–58, doi:10.1175/0065-9401(2003)029<0049:CSVOHT>2.0.CO;2.